Observation of Shot Noise Suppression at Optical Wavelengths in a Relativistic Electron Beam

Daniel Ratner and Gennady Stupakov
SLAC National Accelerator Laboratory, Menlo Park, California 94025, USA
(Received 10 April 2012; published 16 July 2012)

Control of collective properties of relativistic particles is increasingly important in modern accelerators. In particular, shot noise affects accelerator performance by driving instabilities or by competing with coherent processes. We present experimental observations of shot noise suppression in a relativistic beam at the Linac Coherent Light Source. By adjusting the dispersive strength of a chicane, we observe a decrease in the optical transition radiation emitted from a downstream foil. We show agreement between the experimental results, theoretical models, and 3D particle simulations.

DOI: 10.1103/PhysRevLett.109.034801 PACS numbers: 29.27.−a, 29.20.−c, 41.60.Cr

Understanding and controlling collective interactions in relativistic beams is vital for new applications of ultrabright particle sources such as x-ray free electron lasers (FELs) [1,2]. In FELs, shot noise provides the start-up radiation for self-amplified spontaneous emission (SASE) but also drives the potentially hazardous microbunching instability that can impede coherent processes [3–10]. In seeded FELs, shot noise competes with external modulations during the amplification process [11,12], and suppressing the SASE start-up could extend seeded FELs to x-ray wavelengths. In harmonic seeding schemes such as high gain harmonic generation or echo-enabled harmonic generation [13–15], even reducing shot noise at the initial seed wavelength would lower the seed laser power requirement. Shot noise suppression may also aid other areas of accelerator physics, for example, increasing efficiency in cooling relativistic beams [16,17]. In general, improved understanding and control of shot noise will aid in the design of future SASE FELs, and the microbunching instability itself may prove useful as a novel radiation source [18].

Shot noise suppression at long wavelengths was observed in microwave tubes as early as the 1950s [19], and more recently, similar effects (though from different physics) have emerged in semiconductor devices [20]. In the last few years, several groups have independently proposed suppressing shot noise at short wavelengths in high energy electron beams [17,21–23].

In this Letter, we present the first experimental evidence of optical shot noise suppression in relativistic electrons. Using the scheme of Ref. [23], we demonstrate that matching the beam's collective Coulomb forces to dispersion experienced by the particles in a subsequent magnetic system reduces broad-bandwidth shot noise current fluctuations. We observe this noise suppression through a decrease in optical transition radiation (OTR) emitted by the beam.

To quantify the density fluctuations at a wave vector k we define the noise factor

$$F(k) \equiv \frac{1}{N}\sum_{j,l} e^{ik(z_j - z_l)}, \tag{1}$$

where the double sum is over all N electrons in the beam, and z_j is the longitudinal position along the bunch of the jth electron. We can equivalently define the noise factor as $F(k) = N|b(k)|^2$, with the bunching factor $b(k) \equiv \sum_j \exp[ikz_j]/N$ closely related to the discrete Fourier transform of the electron beam density. We select $F(k)$ as a noise metric because of its relevance to numerous accelerator applications, notably undulator radiation.

If the positions of electrons in the bunch are uncorrelated (i.e., a shot noise distribution), the $N(N-1)$ random phases with $j \neq l$ in Eq. (1) will average to zero. (We assume the wavelengths of interest, $\lambda \equiv 2\pi/k$, are much shorter than the bunch length.) We then find the expected noise factor for shot noise: $F(k) = 1$. If instead the electrons are grouped into microbunches spaced by λ (e.g., in an FEL at saturation), then all N^2 terms in Eq. (1) add in phase, and the noise factor reaches a maximum value of $F(k) \approx N$. In the opposite limit (i.e., noise suppression), the electrons are distributed evenly within a length scale λ. In the ideal case, the phases cancel perfectly, and we find $F(k) = 0$. In reality, one can expect suppression below the shot noise level, i.e., $F(k) < 1$.

Suppressing shot noise is equivalent to creating a beam with anticorrelated particle positions. Developing longitudinal anticorrelations requires both a mechanism for particle-particle interactions and a mechanism for subsequent displacement in z. In a relativistic beam, the longitudinal velocity of all particles is close to the speed of light, so relative velocity differences between particles are small. To facilitate longitudinal displacements, Ref. [23] proposed the following noise suppression setup: in an interaction region of length L_a, Coulomb repulsion changes the particle energies, and a subsequent magnetic chicane of dispersive strength R_{56} then shifts the longitudinal particle positions according to the new energies. The simplified model of [23] assumes that the particles are longitudinally frozen in the interaction region (i.e., the velocity differences are small compared to the effect of the chicane strength) and that there is negligible energy change through the dispersive region. For a beam with uniform transverse

density, the noise factor at the exit of the chicane can be written as

$$F(k) \approx (1 - \Upsilon)^2, \tag{2}$$

where

$$\Upsilon \equiv n_0 R_{56} A \quad \text{and} \quad A \equiv \frac{4 r_e L_a}{a^2 \gamma}, \tag{3}$$

with longitudinal particle density (number of particles per unit length) n_0, classical electron radius r_e, relativistic factor γ, and transverse beam radius a. Choosing R_{56} to set $\Upsilon = 1$ reduces the noise factor, $F(k)$, to zero. While the results of Ref. [23] were based on a 1D model, Ref. [24] shows that 1D and 3D models produce nearly identical noise factors for flattop transverse distributions.

We can repeat the analysis for a transverse Gaussian distribution of rms size σ, producing a transversely integrated noise factor

$$F(k) \approx 1 - 2\Upsilon + \tfrac{4}{3}\Upsilon^2, \tag{4}$$

where in Eq. (3) we now replace a by 2σ [24]. For the Gaussian case, we expect optimal shot noise suppression with $\Upsilon = 3/4$, giving $F(k) = 1/4$.

The results of Eqs. (2) and (4) are both valid only in the high frequency regime of $k\sigma/\gamma \gg 1$ [25], when the transverse dimension is large compared to the wavelength of interest in the beam rest frame. In this Letter, the experimental conditions do not strongly satisfy the high frequency limit, so we expect moderate deviations from the analytical results. We note that narrow bandwidth noise suppression is possible even when $k\sigma/\gamma \lesssim 1$.

For an experimental demonstration of shot noise suppression, we use the first linac and bunch compressor sections of the Linac Coherent Light Source (LCLS). The experiment includes the four components shown in Fig. 1: two dipole magnets and the "QB" quadrupole which reset the beam to an initial shot noise distribution, an interaction region which includes the S-band ($L1S$) and X-band ($L1X$) accelerator sections, a dispersive region consisting of a magnetic bunch compressor chicane (BC1), and a diagnostic station. The rf accelerator phase is set to 0° in $L1S$ and 180° in $L1X$ to minimize energy variation along the bunch. Table I gives the main beam and accelerator parameters.

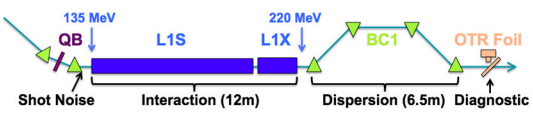

FIG. 1 (color online). Schematic of the LCLS beam line used in the experiment, including the QB quadrupole, $L1S$ and $L1X$ accelerator sections, and bunch compressor chicane BC1. A camera collecting radiation from the OTR foil serves as the diagnostic.

TABLE I. Parameter list for experimental conditions.

Beam energy	135–220 MeV
Beam charge	5–20 pC
Normalized emittance (x, y)	0.2 μm
BC1 dispersion (R_{56})	0–2.5 mm
QB strength	10.3 kG
Interaction beam size (σ)	30–200 μm
OTR beam size (σ_{OTR})	25–40 μm
Camera bandwidth (λ)	400–750 nm
Camera aperture (θ_{cam})	75 mrad

Previous studies found that setting the QB quadrupole to its nominal value (which makes an achromatic transition through the two bend magnets) allows a microbunched beam to enter the interaction region [5]. To suppress this microbunching and prepare a clean shot noise beam, we set the quadrupole off achromat by 3% of its nominal strength. This creates R_{51} and R_{52} transfer elements that wash out longitudinal modulations originating in the injector [8]. Figure 2 shows the off-achromat setting produces a linear variation in OTR intensity as a function of charge, confirming an initial shot noise distribution at the start of the experimental region.

Coulomb repulsion between electrons changes the particle energies as the beam passes through the accelerator segments $L1S$ and $L1X$. The dispersion from the bunch compressor chicane, BC1, then converts the energy modulation into longitudinal displacement, reducing shot noise density fluctuations. Ideally, the particles would have negligible relative longitudinal movement in the interaction region ($L1S$ and $L1X$) and would have negligible interaction in the dispersive region. To check the first assumption, we calculate the effective R_{56} of $L1S$ and $L1X$ due to velocity differences between particles. By operating in low charge mode (5 pC), the R_{56} of optimal suppression (approximately 1.5 mm) is large compared to the effective R_{56} of $L1S$ and $L1X$ (approximately 0.1 mm). We also

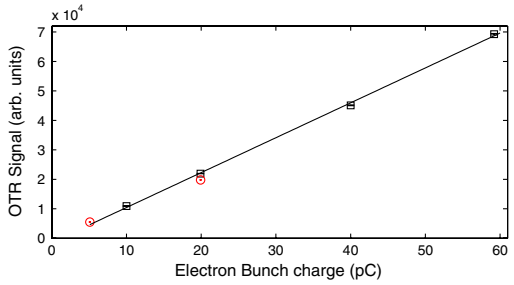

FIG. 2 (color online). Measured OTR intensity as a function of electron beam charge with the QB quadrupole set 3% off achromat and $R_{56} = 0$ mm. A linear fit (solid line) confirms that the measured OTR scales linearly with bunch charge, as expected for a shot noise distribution. Red circles correspond to the $R_{56} = 0$ mm data points in Fig. 4 and are consistent with an initial shot noise distribution. In all figures, error bars fall within the data points.

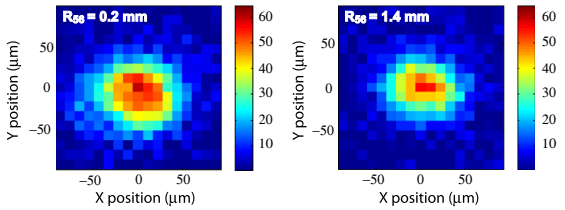

FIG. 3 (color online). OTR images averaged over 100 shots with shot noise properties at $R_{56} = 0.2$ mm (left) and noise suppression when $R_{56} = 1.4$ mm (right). Pixel counts are in arbitrary units.

check that the interaction length, L_a, is long compared to the drift length required for a quarter plasma oscillation, $Z_{1/4}$ (see, e.g., [26]); at 5 pC charge, the average quarter plasma length is $Z_{1/4} \sim 80$ m. Finally, we note that the experimental configuration loosely satisfies the second assumption; the chicane length (6.5 m) is approximately half the length of the interaction region (12 m). Moreover, because half of the dispersion is in the initial 2.5 m of the chicane, the additional interaction in BC1 is a relatively minor effect. Corrections to both assumptions serve only to shift the point of optimal noise suppression to smaller R_{56}.

We measure the OTR emitted from a 1 μm thick aluminum foil inserted into the beam following BC1 [27]. A camera with an aperture of 75 mrad images the OTR screen, and we integrate over the 2D image to calculate the total signal. The radiated energy per unit solid angle per unit wave number observed at angle θ is

$$\frac{d^2I}{dkd\Omega} = \frac{r_e mc^2}{\pi^2} \frac{\theta^2}{(\theta^2 + \gamma^{-2})^2} \sum_{j,l} e^{ik[\theta(r_j - r_l) + z_j - z_l]}, \quad (5)$$

with electron mass m, speed of light c, and transverse particle positions r (see, e.g., [28]). We note that by setting either $\theta = 0$ or $r = 0$, the sum in Eq. (5) reduces to $F(k)$ [Eq. (2)]. In using OTR as a diagnostic, we collect radiation at angles $\theta \neq 0$, so the experimental signal is affected by the transverse phase factors $e^{ik\theta(r_j - r_l)}$, and we expect the measured OTR to differ from the expression for $F(k)$.

After setting BC1 to the optimal R_{56}, we observe shot noise suppression for both 5 and 20 pC electron bunches. Figure 3 shows averaged OTR images for conditions with shot noise ($R_{56} \sim 0.2$ mm) and optimal noise suppression ($R_{56} = 1.4$ mm). The optimal R_{56} for noise suppression is far weaker than the nominal set point ($R_{56} \sim 40$ mm), so during normal LCLS operation we expect only noise amplification.

Scanning the R_{56} of BC1, Fig. 4 shows maximum OTR suppression of 35% at 5 pC and 25% at 20 pC. For both charges, the OTR intensity varies quadratically in R_{56} as predicted by Eq. (4). The point of maximum suppression is determined by the parameter Υ, which is proportional to the longitudinal density n_0. The density varies linearly with bunch charge, so we expect the R_{56} of maximum noise

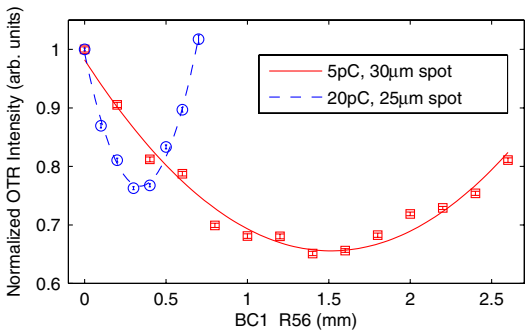

FIG. 4 (color online). Integrated OTR intensity vs R_{56} of BC1. Both the 20 (blue circle) and 5 pC (red square) measurements are fit to quadratic curves (solid lines). In each curve, the intensities are normalized by the measured signal at $R_{56} = 0$ mm.

suppression to vary inversely with bunch charge. Figure 4 confirms that decreasing the bunch charge from 20 to 5 pC results in a corresponding increase in optimal R_{56}. The weaker suppression in the 20 pC case may be partially due to plasma oscillations; with $Z_{1/4}$ a factor of two smaller than at 5 pC, the OTR at $R_{56} = 0$ mm may itself be below the shot noise level as predicted in Ref. [21]. We note that in Fig. 2, the 20 pC point falls approximately 10% below the shot noise level, consistent with the plasma oscillation explanation.

As discussed previously, the transverse components in Eq. (5) can affect OTR emission. In particular, the transverse phase in the exponent of Eq. (5) washes out collective effects at angles $\theta_{\max} > \lambda/(2\pi\sigma_{\mathrm{OTR}})$, with σ_{OTR} the electron beam size at the OTR screen. As a result, measured suppression in OTR is expected to be smaller than the suppression of the longitudinal noise factor $F(k)$ predicted by Eq. (4). Because the camera system images the OTR foil, it is not possible to separate out the contribution from angles smaller than $\theta_{\max}$. However, focusing to smaller σ_{OTR} leads to larger $\theta_{\max}$, and the measured OTR signal better approximates $F(k)$.

Figure 5 shows noise suppression at 20 pC bunch charge for two different beam sizes at the OTR foil. By controlling σ_{OTR} using only quadrupoles downstream of $L1S$ and

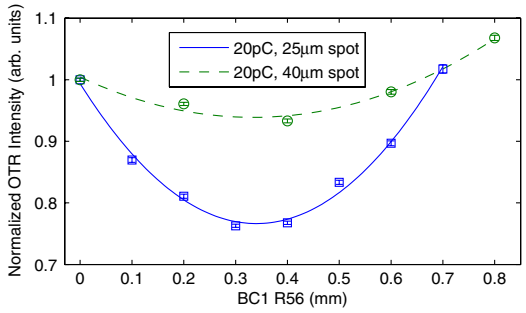

FIG. 5 (color online). Integrated OTR intensity vs beam size at the OTR foil. Both curves are for 20 pC bunch charge, and the lines are quadratic fits.

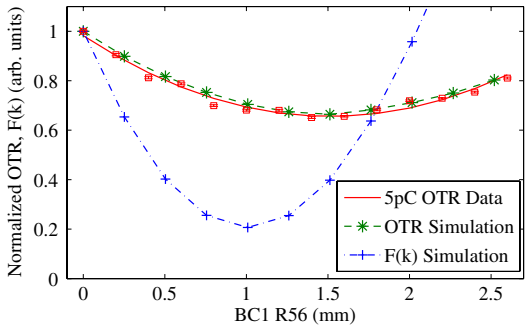

FIG. 6 (color online). Simulation results compared to the experimental data for the 5 pC case. Due to uncertainty of beam size, we fit the beam density to best match the experimental results, producing the curve with green stars for $\sigma = 60$ μm. All other parameters are taken from Table I. The same simulation suggests we have considerably stronger suppression of $F(k)$.

$L1X$, we ensure that the beam size in the interaction region does not change. We then expect that the suppression in $F(k)$ is equal in both cases, and the observed difference between the two curves in Fig. 5 is due to the radial parts of the phase factors in Eq. (5). We note that even with the reduced beam size, coherent effects are damped at angles larger than $\theta_{\max} \sim 2/\gamma$, while the OTR camera integrates over an angle of $\theta_{\text{cam}} \approx 30/\gamma$.

We use 3D particle simulations to confirm both the analytical model and experimental results. To simulate generic interaction and dispersion examples, we developed a custom code that sums interparticle Coulomb forces, and then calculates both the $F(k)$ [Eq. (1)] and the OTR intensity [Eq. (5)] following a chicane. Particles are longitudinally stationary during the interaction and transversely stationary throughout. We assume a longitudinal flattop distribution with periodic boundary conditions and a Gaussian transverse distribution. Due to computational constraints, we cannot simulate the full electron beam, so we use lower particle densities, n_0, and scale R_{56} accordingly.

From the parameters of Table I and the analytical model of Eq. (4), we estimate a 5 pC Gaussian beam will have maximum noise factor suppression for $R_{56} \sim 1.1$ mm, with OTR suppressed at somewhat longer wavelengths due to the transverse components of Eq. (5). Using the same parameters, the simulations predict optimal noise factor suppression at 1.4 mm and optimal OTR suppression at 1.7 mm. The analytical model predicts smaller optimal R_{56} values due to the assumption of the high frequency limit, $k\sigma/\gamma \gg 1$, which is not strongly satisfied by the experimental parameters, for which $k\sigma/\gamma < 2$. As expected, suppression of $F(k)$ is more dramatic than suppression of OTR. Again, the simulation results differ somewhat from the model (factor of 5 suppression in simulation, factor of 4 in the model) due to the assumption of the high frequency limit in the analytical calculations.

Figure 6 shows that both simulations and the analytical model agree reasonably well with experimental results. Because the R_{56} of optimal suppression depends on both the current density and transverse distribution, neither of which can be measured directly in the interaction region, we fit the simulation density to match the experimental R_{56} of optimal suppression. We find that the simulations match the experimental results with a density 25% larger than reported in Table I, which is within the experimental uncertainty. Figure 6 suggests that suppression of $F(k)$ may be considerably stronger than the measured suppression of OTR.

We conclude that we have observed suppression of optical shot noise in a relativistic electron beam. We are able to suppress OTR intensity by as much as 35% of the shot noise level. We find good agreement between the experiments, analytical model, and 3D simulations. From Eq. (5) as well as simulation results, we expect that the noise factor is suppressed more strongly than the observed OTR. We note that the method described in this Letter may be used to control SASE start-up at the LCLS by using a dispersive region near to the undulators; studies for such an experiment are under way. It is our hope that control of collective properties in relativistic beams will find wide ranging applications in accelerator physics.

We thank F. J. Decker, Y. Ding, P. Emma, M. Gibbs, Z. Huang, S. Kalsi, H. Loos, A. Marinelli, Y. Nosochkov, J. Turner, and J. Wu for helpful discussions and suggestions. Work is supported by Department of Energy Award No. DE-AC02-76SF00515.

Note added.—Following submission, the authors of Ref. [22] have reported similar noise suppression results using the plasma oscillation method [29].

[1] P. Emma *et al.*, Nature Photon. **4**, 641 (2010).
[2] H. Tanaka, in *Proceedings of IPAC2011, San Sebastian, Spain, 2011* (European Physical Society, San Sebastian, Spain, 2011).
[3] E. L. Saldin, E. A. Schneidmiller, and M. V. Yurkov, Nucl. Instrum. Methods Phys. Res., Sect. A **490**, 1 (2002).
[4] Z. Huang and K. J. Kim, Phys. Rev. ST Accel. Beams **5**, 074401 (2002).
[5] R. Akre *et al.*, Phys. Rev. ST Accel. Beams **11**, 030703 (2008).
[6] M. Borland *et al.*, Nucl. Instrum. Methods Phys. Res., Sect. A **483**, 268 (2002).
[7] S. Heifets and G. Stupakov, Phys. Rev. ST Accel. Beams **5**, 054402 (2002).
[8] D. Ratner, A. Chao, and Z. Huang, in *Proceedings of the 2008 Free Electron Laser Conference* (Elsevier, New York, 2008).
[9] Z. Huang *et al.*, Phys. Rev. ST Accel. Beams **13** 020703 (2010).
[10] A. Marinelli and J. B. Rosenzweig, Phys. Rev. ST Accel. Beams **13**, 110703 (2010).

[11] E. L. Saldin, E. A. Schneidmiller, and M. V. Yurkov, Opt. Commun. **202**, 169 (2002).
[12] Z. Huang, in *Proceedings of the 2006 FEL Conference* (Elsevier, New York, 2006), p. 130.
[13] L. H. Yu, Phys. Rev. A **44**, 5178 (1991).
[14] I. Ben-Zvi, L. F. Di Mauro, S. Krinsky, M. G. White, and L. H. Yu, Nucl. Instrum. Methods Phys. Res., Sect. A **304**, 181 (1991).
[15] G. Stupakov, Phys. Rev. Lett. **102** 074801 (2009).
[16] A. A. Mikhailichenko and M. S. Zolotorev, Phys. Rev. Lett. **71**, 4146 (1993).
[17] V. Litvinenko, in *Proceedings of the 2009 FEL Conference* (Elsevier, New York, 2009).
[18] E. A. Schneidmiller and M. V. Yurkov, Phys. Rev. ST Accel. Beams **13**, 110701 (2010).
[19] C. Cutler and C. Quate, Phys. Rev. **80**, 875 (1950).
[20] C. W. J. Beenakker and M. Büttiker, Phys. Rev. B **46**, 1889 (1992).
[21] A. Gover and E. Dyunin, Phys. Rev. Lett. **102**, 154801 (2009).
[22] A. Nause, E. Dyunin, and A. Gover, J. Appl. Phys. **107**, 103101 (2010).
[23] D. Ratner, Z. Huang, and G. Stupakov, Phys. Rev. ST Accel. Beams **14**, 060710 (2011).
[24] D. Ratner, SLAC Report No. SLAC-R-992, 2012.
[25] M. Venturini, Phys. Rev. ST Accel. Beams **11**, 034401 (2008).
[26] K. J. Kim and R. Lindberg, in *Proceedings of the 2011 FEL Conference* (Elsevier, New York, 2011).
[27] H. Loos *et al.*, in *Proceedings of the 2008 Free Electron Laser Conference* (Elsevier, New York, 2008).
[28] A. Chao and M. Tigner, *Handbook of Accelerator Physics and Engineering* (World Scientific, Singapore, 2006).
[29] A. Gover, A. Nause, and E. Dyunin, *Proceedings of the Fourth Microbunching Instability Workshop, College Park, MD, 2012* (to be published).